Automatic Recognition and Segmentation of Overlapped GPR Target Signatures

Qiuyang Ren[1,*], *Yanhui Wang*[1], and *Quang P. Ha*[2]

[1]School of Traffic and Transportation, Beijing Jiaotong University, Beijing 100044, China
[2]University of Technology Sydney, 15 Broadway, Ultimo NSW 2007, Australia

Abstract. Ground penetrating radar (GPR) has been widely utilized for non-destructive inspection of civil infrastructure systems such as bridges and tunnels. However, the identification of GPR signatures poses significant challenges due to the overlapped multiple objects. To overcome the obstacle, we proposed an innovative Mask R-CNN based network considering spatial relationship between GPR signatures. Firstly, to capture the spatial relationship of overlapping signatures, we introduced an improved intersection over union considering central distance and aspect ratio between GPR signatures. Secondly, we further modified the Non-Maximum Suppression and enhanced the corresponding anchor generative mechanism. To validate the proposed method, we conducted testing on GPR scans obtained from real data from a bridge. The results demonstrate that the proposed method not only accurately detects GPR signatures, but also significantly outperforms existing Mask R-CNN in terms of segmenting overlapped GPR signature. Specially, the proposed method achieved an average accuracy of 46.8% in the segmentation task, marking a substantial advancement in the field.

Keywords: Ground penetrating radar, Detection, Segmentation, Mask R-CNN

1 Introduction

Ground Penetrating Radar (GPR) represents a sophisticated advancement in non-destructive testing technologies [1, 2]. This technology finds application in a diverse array of contexts, including the localization of rebar, assessing crack in pavement, and construction quality control [3–5]. GPR operates by emitting short electromagnetic pulses into the subsurface, which propagate in a conical shape, and detecting signals reflected back from objects that possess distinct electromagnetic pulses properties compared to the surrounding medium. However, radar signals are subject to reflection, refraction, and other phenomena, leading to overlapping signatures in scan images. As such, there is a critical demand for automated methods for the identification and segmentation of GPR signature, which is of paramount importance in both scientific research and practical applications [6].

Considering the deep learning (DL) method attracts more attention, automatic GPR image interpretation using DL methods has been the current trend [7]. To segmentate GPR signature, some research tends to use advanced technology based on Mask R-CNN [8]. Qin et al. proposed an automatic detection idea for GPR signals characterizing tunnel lining elements in GPR images by integrating Mask R-CNN [9]. Hou et al. further enhanced the Mask R-CNN with a novel loss function and achieved an average accuracy of 47.64% in the segmentation task [10]. Liu et al. describes a Mask R-CNN based network that automatically detects and segments small cracks in asphalt pavement at the pixel level [11].

Mask R-CNN is built upon the Faster R-CNN architecture [12]. The architecture consists of three phases. The first phase is to input an original image into a pretrained neural network and obtain the corresponding feature map. In the second phase, the Regional Proposal Network (RPN) generates a large number of proposals that are not related to the object category. The final R-CNN stage uses RoIAlign to extract features for each proposal and conducts three tasks: proposal classification, Bbox regression, and mask prediction. At this stage, Non-Maximum Suppression (NMS) plays a crucial role. It filters out multiple, overlapped bounding boxes, retaining only the most promising ones for each object. However, there is a main challenge in segmentation task using Mask R-CNN based network. Traditional NMS primarily focuses on the overlap between Bboxes, as measured by the Intersection over Union (IoU) [13].It does not consider the spatial relationship between the boxes, such as their relative distances or alignment. NMS might discard important detections if their Bboxes overlap significantly, especially when objects of the same class are located close to each other. In the domain of GPR signature identification, particularly in the context of real-world, a prevalent challenge is the presence of the overlapped multiple objects. Thus, the NMS is needed to be modified.

In this paper, to solve the problem of identifying overlapped objects, we firstly introduced an improved IoU by

*Email: 22110306@bjtu.edu.cn

considering the central point distance and aspect ratio between Bboxes. Secondly, based on improved IoU, we further modified the mechanism of NMS in anchor box suppression mechanism in the RPN network to improve the detection effect of overlapping targets.

The remainder of this paper is organized as follows. Section II provides an overview of the proposed method. Section III presents a detailed description of the experiment. Section IV validates the proposed method. Finally, Section V concludes this paper.

2 Methodology

2.1 Overview of Mask R-CNN

The workflow of Mask R-CNN begins with an input image being processed to extract a feature map. From this feature map, a Region Proposal Network (RPN) generates potential object proposals. These proposals are then passed through a Region of Interest (RoI) Align layer, which is used for accurate classification and bounding box (Bbox) regression. At this stage, the NMS streamlines the detection by eliminating redundant bounding boxes that significantly overlap, ensuring that only the highest-scoring boxes for each detected object are retained. In parallel with the classification and bounding box regression, the mask head in the network performs pixel-level classification, predicting the likelihood of each pixel belonging to an object. The detailed structure is in [14].

2.2 Distance guided Non-Maximum Suppression

As an instance-level segmentation algorithm, Mask R-CNN relies heavily on accurate bounding box (Bbox) regression. Studies have shown that the Intersection over Union (IoU) metric can help refine Bbox predictions [15]. IoU, as defined in Eq. (1), is calculated between the predicted Bbox, A, and the ground truth (GT) Bbox, B. While widely used, IoU does not always fully reflect the accuracy of predicted Bboxes. For instance, as illustrated in the center of Fig. 1, IoU cannot differentiate between the accuracy of Bboxes P3 and P4, although P3 is clearly closer to the GT Bbox. To address this limitation, the Generalized IoU (GIoU) was introduced, as given in Eq. (2). In GIoU, the smallest enclosing Bbox, C, that contains both A and B, is used for calculation, where C is generally similar in scale to A and B. However, in simpler overlap scenarios, such as those in the left part of Fig. 1, Bboxes P1 and P2 yield identical IoU and GIoU values despite their evident differences in alignment. To further mitigate these limitations, Hou introduced Directional IoU (DIoU), which incorporates the center distance (CD) between predicted and GT Bboxes [10]. DIoU is formulated in Eq. (3), where CD is computed as the L2 norm within the smallest enclosing Bbox, C.

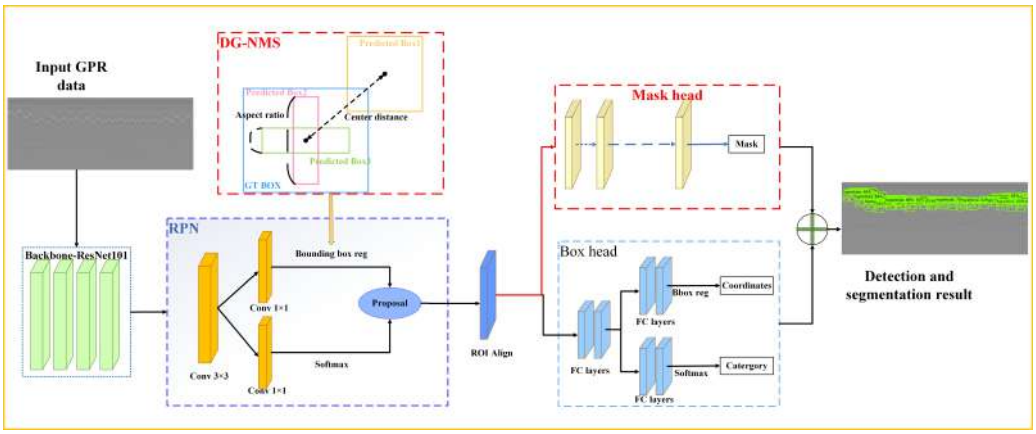

Figure 1: Workflow of Mask R-CNN

$$IoU = \frac{|A \cap B|}{|A \cup B|} \tag{1}$$

$$GIoU = k1 * IoU - k2 * \frac{|C - A \cup B|}{|C|} \tag{2}$$

$$DGIoU = k1 * IoU - k2 * \frac{|C - A \cup B|}{|C|} - k3 * CD \tag{3}$$

However, DGIoU does not account for differences in the aspect ratio of Bboxes, as demonstrated in the right part of Fig. 2, where Bboxes P5 and P6 have identical values for C and CD but differ significantly in aspect ratio. The aspect ratio of a bounding box is defined as the ratio of its width to its height and plays a crucial role in accurately identifying GPR targets, especially when these targets exhibit elongated or hyperbolic shapes (such as rebar). The importance of the aspect ratio lies in its ability to describe the geometry of the detected object, making it a valuable metric for distinguishing between closely overlapping objects. For instance, in the case of rebar detection, the hyperbolic reflection patterns often form elongated bounding boxes, and capturing the correct aspect ratio helps ensure that these objects are accurately localized and segmented.

Figure 2: Similarity comparison of predicted Bbox and GT Bbox using IoU and DGIoU.

To address this, we further propose a modification to DGIoU by incorporating a measure of aspect ratio difference (AR) between the predicted and GT Bboxes. It is calculated in Eq. (4). This measure, AR, quantifies the discrepancy in aspect ratios (ar), thus refining the metric to distinguish between Bboxes more effectively in scenarios where aspect ratio is a critical factor. AR is calculated in Eq. (5).

$$DGIoU_{AR} = k1 * IoU - k2 * \frac{|C - A \cup B|}{|C|} - k3 * CD - k4 * AR \tag{4}$$

$$AR = \frac{4}{\pi^2}(\arctan\frac{x_i + x_r}{y_i + y_r} - \arctan\frac{x_i^2 + x_r^2}{y_i^2 + y_r^2})^2 \tag{5}$$

NMS is a process used to prune multiple Bboxes and use IoU as choosing criteria. Since NMS use IoU as metric, it is natural to altering the mechanism of NMS by combining . The improved NMS can be achieved by simply substitute the standard IoU computation with the improved IoU function wherever the overlap between bounding boxes is assessed.

In summary, the aspect ratio is derived as the ratio of the width (w) to the height (h) of the bounding box, i.e., AR = w/h. This AR metric allows for a more nuanced differentiation of bounding boxes when they overlap, particularly when these targets have a similar central position but different orientations or shapes. By incorporating the aspect ratio into the Non-Maximum Suppression (NMS) algorithm, we improve the localization accuracy of the detected targets, ensuring that GPR signatures, particularly those from closely spaced rebar, are not discarded incorrectly due to minor overlaps. Furthermore, spatial elements, such as the central distance between bounding boxes, also contribute to improving detection. These elements ensure that overlapping targets, which are common in GPR images, are not suppressed purely based on overlap (Intersection over Union, IoU), but instead retain their relevance in the detection process based on their spatial and geometric properties. This combination of aspect ratio and spatial distance refinement enhances the segmentation performance of the Mask R-CNN algorithm when applied to GPR data.

3 Dataset collection

GPR is a sophisticated geophysical technology engineered to investigate subsurface configurations. Its ability to provide detailed images of the subsurface without the need for direct access or excavation has revolutionized the way researchers and professionals investigate the ground beneath our feet.

A typical GPR system comprises several key components: one or more antennas embedded in a control unit, measuring wheel and battery as demonstrated in Fig.3. The brain of the GPR system, the control unit processes the received signals and converts them into visual data that can be analyzed. Measurement wheel can facilitate the movement of the GPR system across a survey area and measure the distance traveled by counting the rotation of the wheels. During operation, the GPR system meticulously scans the subsurface area, with the encoder ensuring precise tracking of the antenna's position.

Integral to the system, the antennae include both a transmitting and a receiving element. The transmitting antenna emits short pulses of electromagnetic energy into the ground, while the receiving antenna captures the signals that are reflected back from subsurface boundaries. As the transmitting antenna emits electromagnetic pulses, two types of waves are generated: a direct or air-wave that travels immediately to the receiving antenna, known as crosstalk, and waves that penetrate the ground which will go into the concrete or soil. And a portion of it will be reflected when the pulse reaches an interface between two media of contrasting dielectric constant. The strength amplitude of the reflected wave at the receiving antenna will be recorded by the system.

A plot of the amplitude versus time for a scan location is an A-scan. A stack of many of those A-scans for a survey line will create an image, which is called a B-scan. As can be seen in Fig. 4, the time on the vertical axis of the B-scan indicates how long it takes for a signal to travel from the transmitting element of the antenna to a pixel location and then back to the receiving element. The horizontal axis shows the distance that the radar moved. A B-scan represents a vertical section perpendicular to the detection surface. The subsurface waves encounter materials with varying dielectric constants, reflecting back when they reach interfaces between materials with different properties.

For this study, we utilized the Impulse Radar CO4080 system equipped with an 800 MHz antenna to collect GPR B-scan images from a bridge in Fig.5. The radar system's scan window was set to 8 ns, with a spatial sampling interval of 0.27 cm and a time sampling interval of 0.016 ns. The scans were carried out along a central survey line on the bridge, aiming to capture a comprehensive range of internal structural information, particularly related to rebar placement. A total of 90 B-scan images were collected, each providing detailed radar reflections that will be used for further analysis. The radar setup was carefully chosen to ensure that it could capture high-resolution data, accounting for the varying depths and potential corrosion of the rebar.

The typical GPR image is collected from the survey line in bridge to verify the effectiveness of proposed methodology. The survey line is located in the middle of the bridge. Fig.6. (a). demonstrated the GPR signature. In this image, it can be observed the target signature has serious overlapped scenario. The output consists of 3 parts, which are

the predicted mask patch (Fig. 6. (b)), and the final detection and segmentation result (Fig. 6. (c)). Fig. 6 (b) shows the mask image on a black background with each individual instance marked with a different colour. Noticed, using different colours to represent masks is just for convenience in showing different instances. Fig. 6. (c) consists the predicted rectangle box, confidence score, and mask patch. It can be found that the intersected targets can also be segmented by the proposed method. Thus, all targets were segmented.

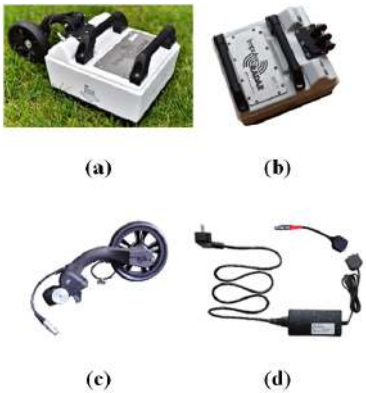

Figure 3: The GPR system. (a). The whole GPR system (b). The control unit. (c). The measurement wheel. (d). The battery

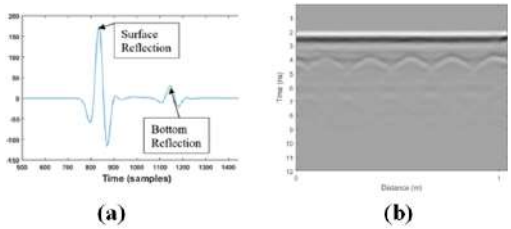

Figure 4: The raw GPR image. (a) A-scan. (b) B-scan.

Figure 5: The demonstration of the bridge.

4 Discussion

4.1 Segmentation results

The typical GPR image is collected from the survey line in bridge to verify the effectiveness of proposed methodology. The survey line is located in the middle of the bridge. Fig.6. (a). demonstrated the GPR signature. In this image, it can be observed the target signature has serious overlapped scenario. The output consists of 3 parts, which are the predicted mask patch (Fig. 6. (b)), and the final detection and segmentation result (Fig. 6. (c)). Fig. 6 (b) shows the mask image on a black background with each individual instance marked with a different colour. Noticed, using different colours to represent masks is just for convenience in showing different instances. Fig. 6. (c) consists the predicted rectangle box, confidence score, and mask patch. It can be found that the intersected targets can also be segmented by the proposed method. Thus, all targets were segmented.

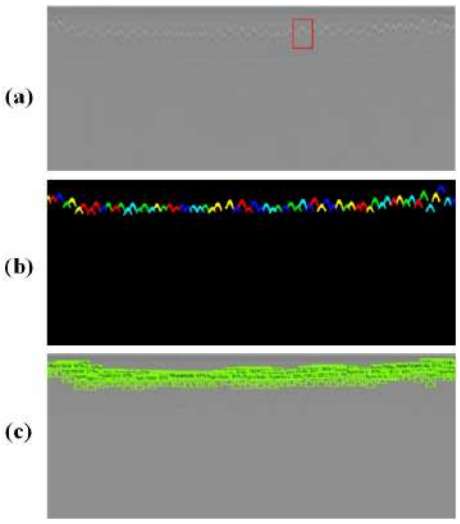

Figure 6: Result of signature detection. (a) Original GPR image; (b) Mask image; (c) Final segmentation results.

4.2 Comparison between different NMS

To test the performance of proposed DG-NMS, the comparison test was performed. We selected the initial NMS and two types of widely used improved NMS for comparison. Similar to DG-NMS, GIoU-NMS and DGIoU-NMS use GIoU and DGIoU as the selection basis for Bboxes in the NMS algorithm.

Fig.7 is the result of segmentation performance. It was found that the mask accuracy improved by using DG-NMS significantly over NMS, GIoU-NMS and DIoU-NMS. In detail, compared to the GIoU-NMS and DIoU-NMS, DIoU-NMS has a relative 1.51% and 1.11% improvement at AP. Notable, the aspect ratio in the DG-NMS could provide the shape information. This is because the GPR signature normally has a shape of hyperbola. And ideally, the coordinates of Bbox can identify three points in the hyperbola which is the vertex and two intersection points with x-axis. Thus, the aspect ratio of Bbox contains a hyperbola can reflect the shape and boundary information to some extent.

The results indicate that DG-NMS outperforms GIoU-NMS and DIoU-NMS in segmentation tasks, suggesting that the directional guidance in DG-NMS, which accounts for spatial arrangement and shape characteristics of GPR signatures, significantly enhances accuracy. In these tasks, the aspect ratio parameter in DG-NMS plays a crucial

role by providing shape-related information specific to GPR signatures. By incorporating both spatial and shape data—through consideration of the aspect ratio and centre distance of GPR signatures—DG-NMS achieves improved localization and segmentation of these signatures.

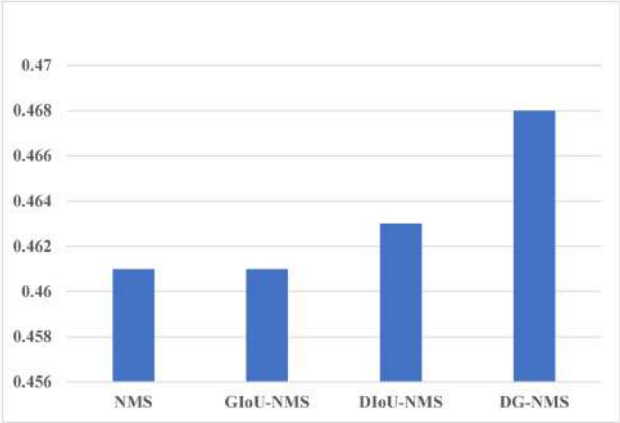

Figure 7: Comparison of different NMS.

5 Conclusion

In this paper, a Mask R-CNN based method is developed to automate the detection and segmentation of GPR signatures. To improve its performance in segmenting overlapped signatures, a modified IoU is proposed and incorporated with NMS as a new strategy to leverage the spatial and shape information by considering both the aspect ratio and centre distance of GPR signatures. The experiment results demonstrated the effectiveness of proposed method in enhancing the performance of Mask R-CNN. The improved Mask R-CNN achieved a segmentation AP of 46.8%.

There are some limitations that could be addressed in future research. The proposed method demands extensive real data for training due to the limited availability of publicly accessible GPR datasets. Future efforts should prioritize the collection and preparation of GPR datasets to facilitate method implementation. Moreover, the method proposed in this article has the characteristics of mask supervision when applied, so it requires a large number of high-precision mask annotations. In the future, we can continue to study methods that do not require mask supervision for the hyperbolic shape characteristics of GPR signals.

References

[1] Alani, A.M. and F. Tosti, GPR applications in structural detailing of a major tunnel using different frequency antenna systems.*Construction and Building Materials*, 2018. 158: p. 1111-1122

[2] Lai, W.W.L., X. Derobert, and P. Annan, A review of Ground Penetrating Radar application in civil engineering: A 30-year journey from Locating and Testing to Imaging and Diagnosis. *Ndt & E International*, 2018. 96: p. 58-78.

[3] Esposito, G., et al., A Deep Learning Strategy for Multipath Ghosts Filtering via Microwave Tomography. Ieee Transactions on Geoscience and Remote Sensing, 2024. 62.

[4] Guo, K., et al., ESTIMATION OF STRESS INTENSITY FACTOR FOR SURFACE CRACKS IN THE FIRTREE GROOVE STRUCTURE OF A TURBINE DISK USING POOL-BASED ACTIVE LEARNING WITH GAUSSIAN PROCESS REGRESSION. Journal of Theoretical and Applied Mechanics, 2024. 62(1): p. 89-101.

[5] Primusz, P., et al., Assessment of In Situ Compactness and Air Void Content of New Asphalt Layers Using Ground-Penetrating Radar Measurements. Applied Sciences-Basel, 2024. 14(2).

[6] Jazayeri, S., et al., Automatic object detection using dynamic time warping on ground penetrating radar signals. Expert Systems with Applications, 2019. 122: p. 102-107.

[7] Lei, W.T., et al., Automatic hyperbola detection and fitting in GPR B-scan image. Automation in Construction, 2019. 106.

[8] Hou, F., et al., Deep Learning-Based Subsurface Target Detection From GPR Scans. Ieee Sensors Journal, 2021. 21(6): p. 8161-8171.

[9] Qin, H., et al., Automatic recognition of tunnel lining elements from GPR images using deep convolutional networks with data augmentation. Automation in Construction, 2021. 130.

[10] Hou, F., et al., Improved Mask R-CNN with distance guided intersection over union for GPR signature detection and segmentation. Automation in Construction, 2021. 121.

[11] Liu, Z., et al., Automatic pixel-level detection of vertical cracks in asphalt pavement based on GPR investigation and improved mask R-CNN. Automation in Construction, 2023. 146.

[12] He, K., et al. Mask R-CNN. in 2017 IEEE International Conference on Computer Vision (ICCV). 2017.

[13] Bodla, N., et al. Soft-NMS - Improving Object Detection With One Line of Code. in 16th IEEE International Conference on Computer Vision (ICCV). 2017. Venice, ITALY.

[14] He, K., et al. Mask R-CNN. in 16th IEEE International Conference on Computer Vision (ICCV). 2017. Venice, ITALY.

[15] Huang, J., et al., A deep learning framework based on improved self-supervised learning for ground-penetrating radar tunnel lining inspection. Computer-Aided Civil and Infrastructure Engineering, 2023